HYDRODYNAMICS ANALYSIS OF DENSITY CURRENTS

H. Afshin*, B. Firoozabadi and M. Rad

Center of Excellence in Energy Conversion, School of Mechanical Engineering
Sharif University of Technology, P.O. Box 11365-9567, Tehran, Iran
h_afshin@mech.sharif.edu – firoozabadi@sharif.edu – rad@sharif.edu

*Corresponding Author

Abstract   Density Current is formed when a fluid with heavier density than the surrounding fluid flows down an inclined bed. These types of flows are common in nature and can be produced by; salinity, temperature inhomogeneities, or suspended particles of silt and clay. Driven by the density difference between inflow and clear water in reservoirs, density current plunges clear water and moves towards a dam, while density current flows on a sloping bed. The vertical spreading due to water entrainment has an important role in determining the propagation rate in the longitudinal direction. In this work, two-dimensional steady-state salt solutions' density currents were investigated by means of experimental studies and data used in turn to verify the numerical model. In the laboratory experiments, the density current enters the channel via a sluice gate, into a lighter ambient fluid and it moves down-slope. Experiments were performed for different concentrations and discharges. Vertical velocity distributions were measured at various stations by Acoustic Doppler Velocimeter (ADV). Results showed a variety of phenomena depending strongly on the entrance buoyancy flux, and Richardson number. As the discharge increases, maximum velocity and current thickness increase as well, but when concentration decreases, the current thickness increases. In the numerical simulation, the governing equations were solved numerically and k-ω turbulence model was used for closure. The buoyancy term was implemented in the numerical model and its constant was calibrated by experiments. For verification, the height and velocity profiles of the dense layer were compared with the experimental data and a good agreement was found.

Keywords   Density Current, k-ω Turbulence Model, Laboratory Experiments, Numerical Modeling

<div dir="rtl">

چکیده   وقتی یک سیال چگال از زیر یک سیال کمتر چگال احاطه کننده، یک سراشیبی را می‌پیماید، جریان چگال به وجود می‌آید. در طبیعت، این نوع جریان معمولاً بر اثر اختلاف چگالی ناشی از اختلاف دما، مـواد محلول و یا ذرات معلق گل و لای به وجود می‌آید. نیروی محرکه این نوع جریان، ناشی از اختلاف چگـالی است. زمانی که جریان چگال روی سطح شیب دار در حال حرکت است، به علت درون آمیختگـی بـا سـیال محیطی، افزایش ارتفاع می‌دهد. درون آمیختگی، نقش مهمی در نرخ گـسترش جریـان چگـال دارد. در ایـن تحقیق، جریان آب – نمک به صورت عددی و آزمایشگاهی مورد بررسـی قـرار گرفتـه اسـت و نتـایج حـل عددی با نتایج تجربی مقایسه شده است. در آزمایشگاه جریان چگال از طریق دریچه ورودی به کانال حاوی آب خالص، وارد می‌شود. آزمایش با غلظت‌ها و دبی‌های مختلف انجام شده است. سرعت نقاط مختلف بـه وسیله دستگاه سرعت سنج داپلر اندازه‌گیری شده است. نتایج نشان می‌دهـد کـه شـکل پروفیـل سـرعت بـه شدت به شار شناوری و عدد ریچاردسون ورودی وابسته است. بـا افـزایش دبـی جریـان ورودی، مـاکزیمم سرعت و ارتفاع جریان افزایش می‌یابد. با کاهش غلظت ورودی نیز ارتفاع جریان افزایش می‌یابـد. در شـبیه سازی عددی جریان چگال، از مدل توربـولانس k-ω اسـتفاده گردیـده اسـت. جملـه شـناوری در معـادلات مومنتوم وارد گردیده و ضریب ثابت با نتایج تجربی کالیبره شده است.

</div>

1. INTRODUCTION

Turbulent density currents are generic features of many environmental flows, whenever a fluid with a certain density flows into a fluid with different density it creates a current. They arise frequently in industrial and natural situations. Whether the density difference is created by temperature, heat, sediment particles or compositional variations, these currents exert a significant influence on transport and dispersion processes. Gravity current is another name for this type of flow. Most density

currents are buoyancy conserving while sediment-laden density currents, which are referred to as turbidity currents, are not. Dynamics of such currents are assumed to be dominated by a balance between inertial, buoyancy, and viscous forces.

Density currents can be seen in atmosphere during thunderstorms, dust storms in deserts, powder-snow avalanches in mountains (Alavian [1]), movement of lavas from erupting volcanoes (Simpson [2]) and gas movements through a mine (Alavian, et al [3]).

Laboratory experiments are useful for visualizing patterns of this behavior even though there are considerable problems in comparing experiments directly with the individual natural density currents. Natural currents vary greatly in size and duration such that any laboratory experiment may represent a subset of natural conditions. The primary advantage of laboratory experiments is that the influence of individual factors can be examined in isolation. This can only be achieved by experimental configurations that greatly simplify the nature of density currents. Such simple experiments are valuable for understanding these processes, but should only be compared with natural case studies with extreme care, particularly in light of problems such as scaling turbulent mixing. Pervious laboratory experiments of density and turbidity currents include Ellison, et al [4], Rad [5], Alavian [1], Garcia [6], Altinkar, et al [7], Kneller, et al [8]. Considerable theoretical (Akiyama, et al [9]) and numerical studies of turbulent density currents have been carried out during the past several decades (Parker [10]; Akiyama, et al [9]; Fukushima, et al [11]; Parker, et al [12]; Choi, et al [13]; Akiyama, et al [14]; Firoozabadi, et al [15], Huang, et al [16]). The incorporation of turbulent kinetic energy in the modeling of density current dynamics is very important. If the turbulent kinetic energy is not properly balanced, a numerical model may predict physically unrealistic acceleration (Parker [10]).

Stacey, et al [17-18] investigated the necessary condition for self-maintenance using a mixing length model for the turbulence closure. Their model allowed for the influence of the current's interface stability on eddy viscosity and diffusivity. Eidsvik, et al [19] applied k-ε turbulence model and investigated the possibility of self-acceleration of the density currents. k-ε model has been adopted by others to simulate two-dimensional density currents in reservoirs (Farell, et al [20]), down an inclined surface in a flow (Firoozabadi, et al [21]; Choi, et al [13]), and recently in submarine channels (Imran, et al [22]). The vertical structure of density currents has also been studied in Brørs, et al [23] by using Reynolds stress model. Using the low Reynolds number turbulent model (k-ε Launder, et al [24]), Firoozabadi, et al [21] investigated the behavior of the various variables of this current and likewise Khakzad, et al [25] used v^2-f turbulence model for investigating the behavior of the density current.

In addition, several researches have been performed on wall jets. Launder, et al [26] have shown that k-ε model is not able to predict the wall jet properly. Also, Ljuboja, et al [27] presented that for a two-dimensional turbulent wall jet, k-ε model associated to wall laws produces a spreading rate more than 30 % higher than the experimental results. They mentioned that k-ε model does not take into account the damping effect of the wall on the lateral velocity fluctuations. Kechiche, et al [28] have mentioned that k-ε model was established for high Reynolds number flows, where viscous effects are negligible compared to the turbulent ones. For wall jets, the viscous layer plays an important role in heat and momentum transfer.

Since the density current is similar and more complex than the wall jet, k-ε model is not suitable for these currents. On the other hand, this current can be classified as the low Reynolds number flows and k-ε model has usually been calibrated and verified for high Reynolds number flows.

The purpose of the present study is to investigate the various characteristics of two-dimensional, steady state, turbulent, non-particulate salt solution density currents, developing on a sloping channel under the strata of clear water. To achieve the detailed characteristics of the density current, a set of laboratory experiments were performed. Then, the experimental data were used to verify the numerical simulation besides other test cases. In this study, the improved k-ω model (Wilcox [29]) was used for turbulence closure. This turbulence model, however, is found to have predicted the characteristics that are in agreement with the experiments.

2. EXPERIMENTAL SETUP

A laboratory apparatus was built to study the two-dimensional flows resulting from the release of the salt solution on a sloping surface in a channel of freshwater. The channel is 12 m long, 0.2 m wide and 0.6 m deep. One side of the channel was constructed of glass for observation purposes. As seen in Figure 1, the channel was divided into two sections along its longitudinal direction by sheets of Plexiglas. The shorter upstream section is an accumulator for dense water with an opening (sluice gate) at the bottom of Plexiglas separator sheet. The opening has a rectangular cross section which was controlled by a gate. The controllable opening allows changing the inlet velocity of the dense water. During the experiments, the opening of the gate was 1 cm high and the ratio of the inlet gate opening to the water depth was about 0.02 (1 cm/60 cm) in order to avoid the recirculation due to stratification. The channel was previously filled with fresh water and its temperature was the same as the laboratory room temperature. As the test began, the dense water continuously left the accumulator through the gate and went down the sloping bottom of the channel. The slope of the

channel bed can be adjusted in the range of 0 % to 3.5 %. The salt solution gradually spread under the fresh water.

Another tank, called reservoir tank, with a maximum capacity of 2 m³ was used to prepare the mixture of the dense water. The reservoir tank was made of stainless steel and was installed at an elevation of 2.5 m from the ground. A supplying pipe fed the dense water from the reservoir into the accumulator. A gate valve controlled the feed rate, and the feed rate was measured by a flow meter and was fixed at a desired rate. Thus, the current was in a quasi-steady condition.

After mixing the salt in the fresh water of the reservoir tank and before feeding it into the accumulator, it was transferred to a weir by another circulation pump. The purpose of using this weir was to keep the dense water head constant and to prevent the impacts of fluctuations in mixing reservoirs on the feed rate.

To avoid the return flow, a 25 cm step was built at the end of the channel as Figure 1 shows. Sixty-four valves were installed at the bottom of the step. The number of the opening valves was dictated by the inlet flow to set the discharge rate, a little more than the inflow rate to let the entrained water out of
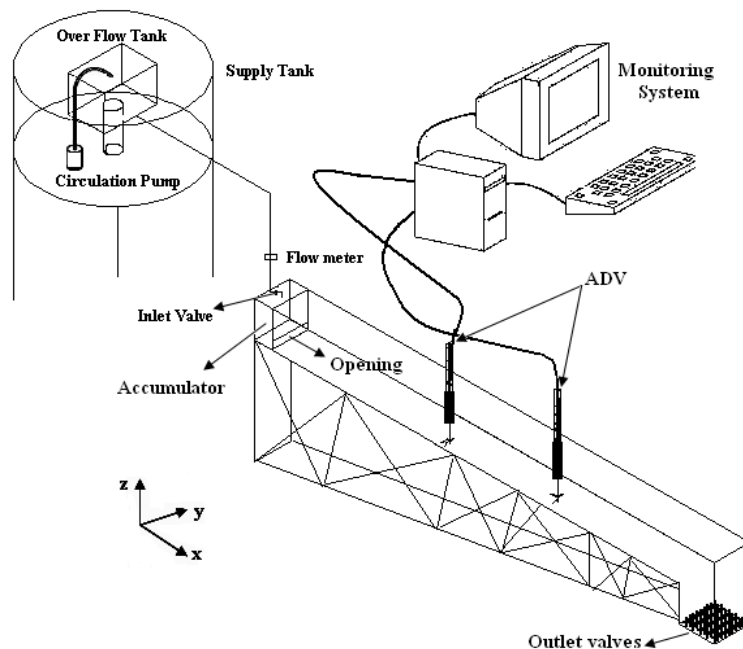

Figure 1. Schematic sketch of the experimental setup.

the channel. To prevent loosing fresh water, we replenished the fresh water at the end of the channel so that the total height of fresh water was kept constant during the experiments. The channels' overflow prevents, over replenishing the fresh water.

Salt with the specific gravity of 1630 kg/m^3 was used as the soluble material for all experiments. Since the initial bulk density of the dense fluid is less than 1008 kg/m^3, the mixture is considered as Newtonian fluid. The velocity profiles were measured by 10 MHz ADV (Acoustic Doppler Velocimeter) made by Nortek Company. The probes of ADV were previously calibrated by the Nortek Company and the measurements have an accuracy of about 0.1 (mm/s).

The distance between the two sensors of this instrument was 1m. The sensors were placed on a rail conveyor of the channel. These two sensors measured the instant velocity at any point in three directions. By changing the vertical location of sensors, the velocity profiles of any specific section were determined. There was a distance of 5cm between the measured points and ADV probe, which did not disturb the flow at those points.

When the head of the current reached the end wall of the basin and the flow reached a steady state, measurements in the body of the current with ADV's began. A steady state condition was achieved when the measuring mean velocities at one point during two minutes were the same. Some seeding material was added to the salt solution to reflect the pulses. The data acquisition took 35-40 s. for each probe's position. The total duration of each experiment was about 80 minutes. These series of experiments were carried out to obtain instantaneous velocities, mean flow properties, and velocity profiles without interfering in the density currents. To find the repeatability of experiments, each run was repeated two times.

3. EXPERIMENTAL RESULTS

After preliminary tests and adjusting the experimental devices and measuring facilities, eleven experiments were performed. For all experiments, the inlet current thickness was set at $h_0 = 1$ cm. The slop of the channel bed was set at 1%. The width of the channel was $b = 20$ cm, thus the inlet velocity $U_0 = Q_0/(b \times h_0)$, where Q_0 is the flow rate. The inlet buoyancy discharge $B_0 = \dfrac{g \cos \theta}{b} \dfrac{\rho - \rho_w}{\rho_w} \times Q_0$ and the inlet Richardson number $Ri_0 = B_0 \big/ U_0^3$ varied as the inlet concentration changed; in which ρ is the density of the mixture, $\rho = C\rho_s + (1-C)\rho_w$, ρ_s and ρ_w are the salt and water density respectively, g is gravity acceleration, C is concentration, and θ is the bed slope. The inlet conditions of these experiments are shown in Table 1. T_{in} denotes the temperature of the saline current in the mixing tank and T_s denotes the temperature of the surrounding water in the channel. The inlet Reynolds number was calculated through $Re_0 = U_0 h_0 / \upsilon$ in which υ is the mixture kinematic viscosity. In Table 1, S is the bed slope of the flume.

Since the inlet Richardson numbers (Ri_0) are adequately lower than unit, the flow at the inlet is supercritical, so the maximum height of the density current occurs close to the inlet.

Considering that one side of the channel is made of glass, we could measure the height by observation. The height of the dense layer was defined as the interface between dyed saline solution fluid and colorless ambient fluid. Hereafter, this height will be called vision height (H_{vision}). Sometimes, in the laboratory, the height of the current was sharp therefore we were convenient to distinguish the interface such as Figure 2a; while in cases such as Figure 2b, the height or interface was not so evident and we had to approximate the vision height.

In the experimental results, the height of the dense layer is shown in Figure 3, it can be seen that as the flow moves down the channel, hydraulic jump occurs and the flow regime changes to subcritical and the height of the density current decreases.

In this study, the effects of changing the parameters including discharge, and concentration on the dense layer height were studied. Figure 3 (a,b,c) shows that the discharge increase, leads to increase of the current height in all concentrations. Also noting Figure 3, from left to right it could be observed that, the increase of concentration causes the current height to decrease.

TABLE 1. Inlet Conditions for Saline Current Experiments.

Run	U_0(cm/s)	C_0 %	B_0(cm^3/s^3)	Ri_0	Re_0	T_{in}(°C)	T_s(°C)
1	12.5	0.5%	39	0.020	1260	21.5	21.5
2	16.7	0.5%	52	0.011	1680	21.5	21.5
3	20.8	0.5%	64	0.007	2100	21.0	21.0
4	25.0	0.5%	77	0.005	2520	21.0	21.0
5	12.5	1%	77	0.040	1260	21.5	21.5
6	16.7	1%	103	0.022	1680	21.5	21.5
7	20.8	1%	129	0.014	2100	21.5	21.5
8	25.0	1%	155	0.010	2520	21.5	21.5
9	12.5	1.5%	116	0.059	1260	21.0	21.0
10	16.7	1.5%	155	0.033	1680	20.5	20.5
11	20.8	1.5%	193	0.021	2100	21.0	21.0
In all experiments: b_0 = 20 cm, h_0 = 1 cm, S = 1 %							
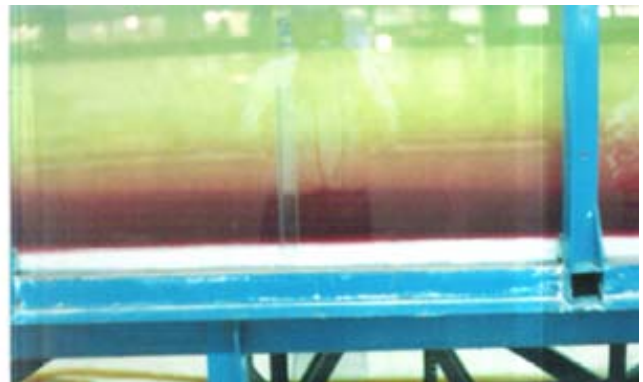
(a)   (b)

Figure 2. Laboratory photos of the density current in Sharif university lab.

Non-dimensional vertical velocity profiles are shown in Figure 4, by moving along the center line of the channel, in the steady state condition and different inlet flow rates and concentrations (buoyancy flux). The distance above the bed is scaled by the inlet thickness and the velocity is normalized with the inlet velocity. The velocity profiles (Figure 4a-k) show a quick increase up to their maximum values at a short distance above the bed. The stream-wise velocity in all runs shows a typical vertical distribution of density driven flow (Garcia [6] and Altinakar, et al [7]).
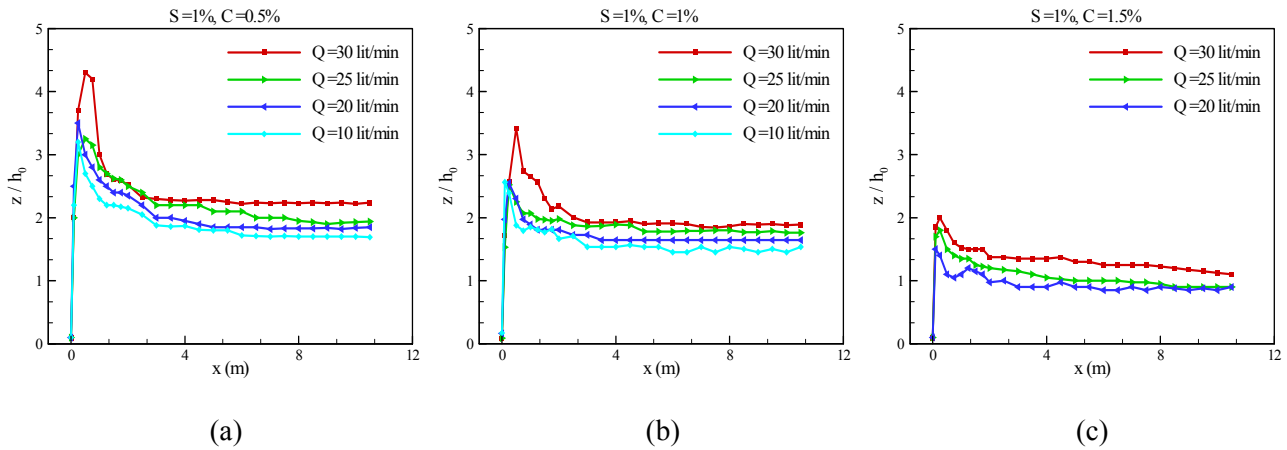
Figure 3. Height of the density current in different inlet concentration and discharge.

It can be seen that as the flow moves down the channel, viscosity causes the inertia forces to decline. Consequently, the maximum and average velocities reduce along the channel. In addition, the maximum velocity shifts upward because of the reduction in driving forces of the density current and also due to the occurrence of maximum shear stress at the bottom. In Figure 4, each row, from left to right, represent the inlet flow rate growth; therefore, the maximum and average velocity at bed level, and also the slope of the velocity increases with the flow rate. The point of maximum velocity shifts upward due to a rise in the inertia force of the entering current and the component of gravity force in the current direction. The magnitude of the shear stress near the bed grows by an increase, in the slope of the velocity profile near the bed, resulting in an increase of the mass flow rate. Each column of Figure 4 represents the increase in the inlet concentration from top to bottom. It can be seen that the maximum and average velocity in the x-direction will rise, from top to bottom, resulting in excessive concentration. It is clear that an increase in the inlet density of the current causes an increase in the driving force as well as the velocity. Besides, with precise observation of the height, of the density current at each column in Figure 4, it can be concluded that an increase in the inlet concentration, leads to a decrease in the height of the dense layer, whose effect is seen in the drop of the concentration profiles (Figure 3).

4. MATHEMATICAL MODELING

4.1. Governing Equations Concentration of dense-water is so small that Bousinesq approximation can be applied; therefore, the effect of density difference is only considered in the buoyancy term, but is neglected in other terms of momentum equations. The equations which describe the motion of a two-dimensional, steady state, turbulent and density current can be expressed as:

$$\frac{\partial u}{\partial x} + \frac{\partial w}{\partial z} = 0 \tag{1}$$

$$u\frac{\partial u}{\partial x} + w\frac{\partial u}{\partial z} = -(\frac{1}{\rho})\frac{\partial p}{\partial x} + g'\sin\theta + \frac{\partial}{\partial z}(\upsilon + \upsilon_t)\frac{\partial u}{\partial z} \tag{2}$$

$$u\frac{\partial w}{\partial x} + w\frac{\partial w}{\partial z} = -(\frac{1}{\rho})\frac{\partial p}{\partial z} - g'\cos\theta + \frac{\partial}{\partial z}(\upsilon + \upsilon_t)\frac{\partial w}{\partial z} \tag{3}$$

$$u\frac{\partial C}{\partial x} + w\frac{\partial C}{\partial z} = \frac{\partial}{\partial z}(\lambda + \zeta_s)\frac{\partial C}{\partial z} \tag{4}$$

These equations are continuity, momentum in x and z directions, and diffusion respectively. u and w are components of the velocity in x and z directions and p is the pressure. C is concentration of the dense layer defined as $C = (\rho-\rho_w)/(\rho_s-\rho_w)$.
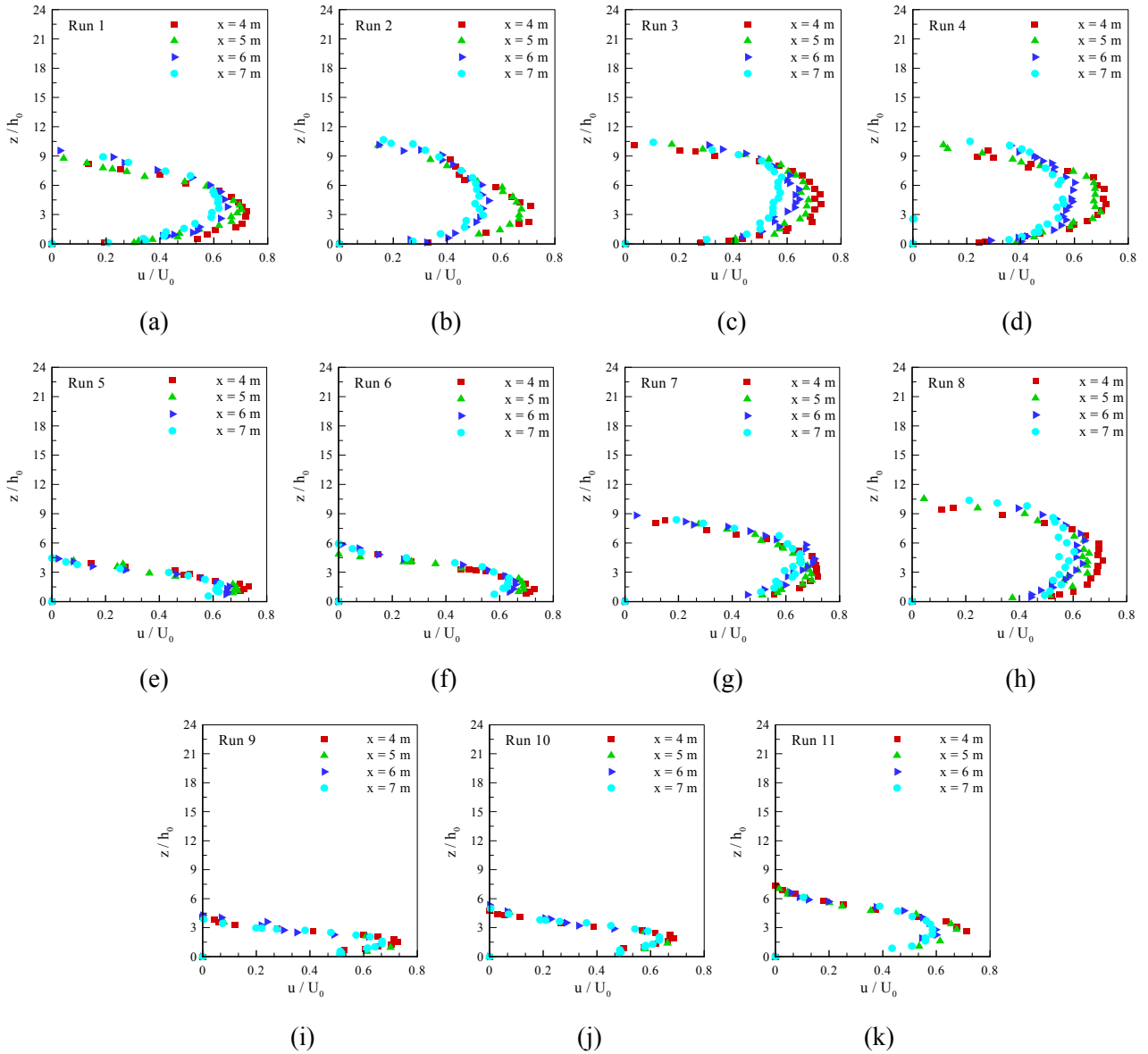
Figure 4. Typical velocity profiles in four different locations at experimental Runs.

The density of the mixture is defined as $\rho = C\rho_s + (1-C)\rho_w$. υ and λ are the viscosity and diffusivity of the fluid respectively. In the momentum equation (Equation 2,3), g' is the reduced gravitational acceleration:

$$g' = g\frac{\rho - \rho_w}{\rho_w} \tag{5}$$

υ_t is the turbulent viscosity and is defined later. In the concentration equation (Equation 4), ξ_s is the turbulence diffusivity. By using the turbulent Schmidt number Sc, the eddy diffusivity is:

$$\zeta_s = \frac{\upsilon_t}{Sc} \tag{6}$$

While Schmidt number, like Prandtl number, is predictably affected by the buoyancy, it is assumed to be at unity here (Lyn, et al [30]). Equations 1-4 are not closed because the eddy viscosity remains unknown. Numerous turbulence models may be

used to estimate the eddy viscosity. Most eddy viscosity based turbulence models, such as the standard k-ε model over predict turbulent kinetic energy in stagnation points (e.g., near the solid boundaries). This weakness probably arises because of the fact that such models have been developed for high Reynolds numbers and isotropic turbulent flows, and therefore cannot accurately simulate the near wall regions where the flow is not isotropic, nor is its Reynolds number high. Herein, k-ω turbulence model is employed to evaluate the eddy viscosity.

4.2. Turbulence Modeling Nowadays, most predictions in industry involve the use of standard or modified versions of the standard k-ε turbulence model. These models have usually been developed, calibrated and validated, using flows parallel to the wall. Physical phenomena involved in the density currents are considerably different and have been considered as highly challenging test cases for the validation of turbulence models. Since, the density current lies close to the bed and has a short height from the bed; the near bed behavior will have an important effect on the characteristics of the current. But, the standard k-ε model showed a poor result in this region (Parneix, et al [31], Lander, et al [24]). Moreover, this current becomes turbulent at rather low Reynolds numbers (order 1000); thus, the standard k-ε model which has been standardized for high Reynolds numbers and isotropic turbulence flow, hence cannot simulate the anisotropy and non-homogenous behavior near the wall (Parneix, et al [31]). In order to integrate k and ε into the wall, it is common practice, to introduce the low-Reynolds number damping functions. These are adjusted by certain behavior near the wall (Launder, et al [24]). However, all these models use a single-point approach (Durbin, et al [32]) that cannot represent the non-local effects of the pressure-reflection that occur near solid boundaries. In many cases, these damping functions involve an ill-defined normal distance to the wall, which cannot be used in complex geometries. They are also highly non-linear, and sometimes introduce numerical rigidity.

An attractive alternative to the standard k-ε model is k-ω turbulence model (Wilcox [29]). There is considerable evidence that k-ω model is stronger computationally, than the standard k-ε

model for the integration of turbulent flows to a solid boundary. The quantity k illustrates a measure of the kinetic energy of turbulence. It is not critically important whether k is identified as the exact kinetic energy of the turbulence or, alternatively, the kinetic energy of the fluctuations in the direction of shear, (Wilcox [29]). The second quantity introduced in the model, ω is referred to as the specific dissipation rate. Its dimensions are inversely proportional to time. Perhaps the simplest physical interpretation of ω is that it is the ratio of the turbulent dissipation rate ε to the turbulent mixing energy. Alternatively, ω is the rate of dissipation of turbulence per unit energy. The relation between ε and ω is defined by:

$$\omega = \frac{\varepsilon}{(c_\mu k)} \tag{7}$$

The turbulent mixing energy for k-ω model is:

$$\frac{\partial}{\partial x_j}(u_j k) = \frac{\partial}{\partial x_j}[\left(\upsilon + \sigma^* \upsilon_t\right)\frac{\partial k}{\partial x_j}]$$
$$+ \frac{\tau_{ij}}{\rho}\frac{\partial u_i}{\partial x_j} + \beta g_i \frac{\upsilon_t}{\sigma_d}\frac{\partial C}{\partial x_i} - c_\mu \omega k \tag{8}$$

Specific dissipation rate is:

$$\frac{\partial}{\partial x_j}(u_j \omega) = \frac{\partial}{\partial x_j}[(\upsilon + \sigma \upsilon_t)\frac{\partial \omega}{\partial x_j} +$$
$$c_{1\varepsilon}\frac{\omega}{k}\left(\frac{\tau_{ij}}{\rho}\frac{\partial u_i}{\partial x_j} + c_{3\varepsilon}\beta g_i \frac{\upsilon_t}{\sigma_d}\frac{\partial C}{\partial x_i}\right) - c_{2\varepsilon}\omega^2] \tag{9}$$

In k-ω model, $\beta g_i \frac{\upsilon_t}{\sigma_d}\frac{\partial C}{\partial x_i}$ is the buoyancy term, υ_t is kinematic viscosity, τ_{ij} is Reynolds stress tensor and β is the volume expansion coefficient. The turbulent mixing energy k and the specific dissipation rate ω are needed to define the turbulence viscosity υ_t, which is given by:

$$\upsilon_t = \gamma\frac{k}{\omega} \tag{10}$$

We invoke Boussinesq approximation that Reynolds

stress tensor is proportional to the mean strain- rate tensor, that is,

$$\frac{\tau_{ij}}{\rho} = \upsilon_t \left[\frac{\partial u_i}{\partial x_j} + \frac{\partial u_j}{\partial x_i} - \frac{2}{3} \frac{\partial u_k}{\partial x_k} \delta_{ij} \right] - \frac{2}{3} k \delta_{ij} \qquad (11)$$

Several closure coefficients, namely, c_μ, $c_{1\varepsilon}$, $c_{2\varepsilon}$, $c_{3\varepsilon}$, γ, σ, σ^*, σ_d appear in the above equation. The values are summarized in the following (Wilcox [29])

$$c_\mu = \frac{9}{100}, \quad c_{1\varepsilon} = \frac{5}{9}, \quad c_{2\varepsilon} = \frac{3}{40},$$

$$\gamma = 1, \quad \sigma = \frac{1}{2}, \quad \sigma^* = \frac{1}{2}, \quad \sigma_d = 1$$

The empirical constant, $c_{3\varepsilon}$ associated with the buoyancy term is uncertain. This constant depends on the slope of the channel (Huang, et al [16]). For horizontal shear flows, the buoyancy term does not affect the flow and should not be considered in Equation 9 and so $c_{3\varepsilon} = 0$, while the buoyancy term should contribute completely in Equation 9 for vertical shear flows; therefore $c_{3\varepsilon} = 1$ (Rodi [33]). Fukushima, et al [34] using k-ε model showed that a value of the $c_{3\varepsilon}$ in the range of 0-0.4 yields good agreement between the numerical solution and experimental results for density currents. In this study, we discussed and performed the numerical tests on the $c_{3\varepsilon}$ constant.

4.3. Geometry Specification and Boundary Conditions
Geometry specification and boundary conditions are listed in Table 2. Sketch of boundary conditions is shown in Figure 5. Test case 1 and 2 are the experimental data presented by Akiyama, et al [9] and test case 3, 4 and 5 are the results of present experiments.

In the present study, various boundary conditions such as the inlet, the bottom, and the free surface boundary condition are required. Known quantities are specified at the inlet for inflow velocity U_0, concentration C_0, and current thickness h_0. Turbulent kinetic energy and dissipation rate at the inlet are estimated, respectively, as $k_{in} = 10^{-4} U_0$ and $\omega_{in} = 10 k_{in}^{0.5} / (c_\mu h_0)$ (Ferziger, et al [35]). At the

free surface, a symmetry boundary condition (no flux condition) is used. This assumption is typically well unless the dynamics of the free surface affects the propagation of the density current, i.e., the overlying depth of the surrounding water is about ten times greater than the current thickness. At the bottom, the no-slip condition is imposed, i.e., $u = v = 0$. For solute concentration, zero flux is used at the bottom, i.e., $\frac{\partial C}{\partial z} = 0$. The turbulence model is invalid in the viscous sub layer, so the law of the wall was applied in the bottom boundary. In this region, the velocity is estimated by using the following wall function:

$$U^+ = \frac{1}{\kappa} \ln y^+ + 5.1 \qquad (12)$$

Where $U^+ = \frac{u}{u^*}$, u^* is shear velocity, κ is von Karman constant and equal to 0.4 and $y^+ = u^* y / \upsilon$. For the turbulence kinetic energy and its rate of dissipation the following relations near the wall are used:

$$k = \frac{u^{*2}}{\sqrt{c_\mu}} \qquad (13)$$

$$\omega = \frac{u^*}{\kappa y \sqrt{c_\mu}} \qquad (14)$$

The no-slip condition at the bottom wall is imposed that k vanishes at y = 0, i.e., k = 0 at $y^+ = 0$.

At the downstream outlet, the flow is assumed to be fully developed; thus, zero gradient for velocity components and concentration are employed, i.e. $\frac{\partial u}{\partial x} = \frac{\partial v}{\partial x} = \frac{\partial c}{\partial x}$.

4.4. Solution Method
The flow and the turbulent equations have to be correctly resolved to obtain concentration distribution predictions. All computations were performed in Cartesian coordinates with rectangular geometry. Cartesian grids were used, with a high resolution near all solid boundaries (Figure 6). The numerical

TABLE 2. Specification of Computational Geometry and Boundary Conditions.

Specification	Test Case 1 Akiyama, et al [14]	Test Case 2 Akiyama, et al [14]	Test Case 3 (Run 1)	Test Case 4 (Run 4)	Test Case 5 (Run 6)
Length of the Channel	6 m	6 m	10 m	10 m	10 m
Height of the Channel	1.3 m	1.3 m	0.6m	0.6m	0.6m
Dense Layer Inlet Height (h_o)	0.04 m	0.05 m	0.01m	0.01m	0.01m
Inlet Velocity (U_0 m/s)	0.063	0.0684	0.125	0.25	0.167
Inlet Concentration	1.2 %	1 %	0.5 %	1.5 %	1 %
Slope	14 %	10 %	1 %	1 %	1 %
Re_0	2538	3438	1260	2520	1680
Ri_0	0.75	0.66	0.02	0.005	0.023
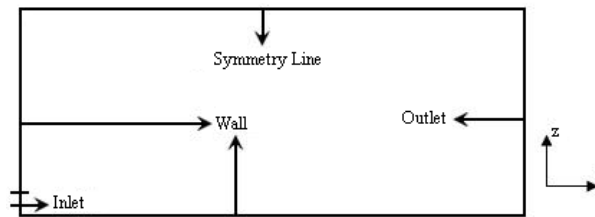
Figure 5. Sketch of boundary conditions.

solution is checked by three-size mesh and the earned results in the two latter size mesh are the same. Therefore the results are grid independent. The final grid is shown in Figure 6.

4.5. Solver This project was solved by an in-house code. The code is to compute two and three dimensional, steady and unsteady, turbulent and laminar flow. The computation is based upon the solution of a partial differential equation, governing the dynamics of the flow. The finite volume method is used to discretize the partial differential equations into an algebraic equation. The tri-diagonal matrix algorithm (TDMA) is applied to solve the obtained algebraic equations. The hybrid scheme was used for discretizing the momentum, turbulence and particles mass balance

equations. The code utilizes the collocated variable arrangement, in which all variables are stored at the same control volume. This means that all the variables are stored at the center of the control volume. This method worked out by Rhie, et al [36] interpolation. SIMPLEC method handles the linking between velocities and pressure. All fluid properties were treated as being constant. The under relaxation coefficient is set at 0.5, 0.8 and 0.3, for velocities, concentration and pressure respectively. Convergence is evaluated for each iteration based on the residual criterion. In this method, the sum of absolute residuals of a variable for all computational control volumes is compared with a reference quantity at the end of each iteration. Here, the inlet flux of each variable is chosen as a reference quantity for the same
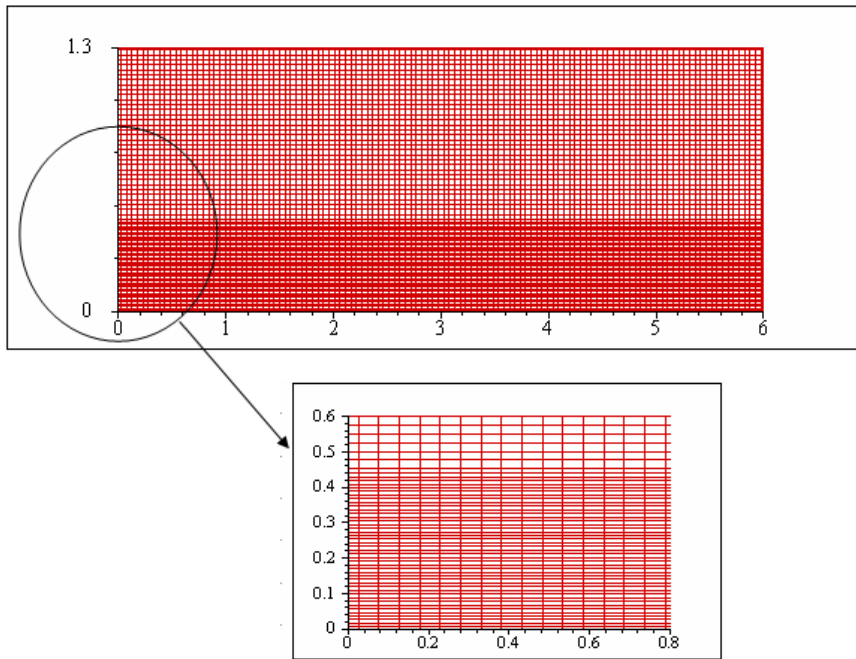
Figure 6. Specification of grids.

variable. When the sum of absolute residuals is normalized by the inlet flux is on the order of 10^{-4} for all variables, computation stops. When iterations are completed, quantities obtained for each variable are saved, and therefore can be used as the basic solution in the next iteration. After velocity components and pressure converge, scalar transport equations for turbulent kinetic energy and dissipation rate are solved. Finally, concentration equation along with all pervious equations is simultaneously solved, and iterations continue until the convergence for all variables is obtained.

5. NUMERICAL RESULTS

5.1. Verification k-ω model has been applied to simulate structure of density current. Hence, the density current was simulated in five test cases. Detailed information for the specification of geometry and boundary conditions has been presented in Table 2. Figure 7 shows the height of the steady density current in comparison with the experimental data presented by Akiyama, et al [9]

for different $c_{3\varepsilon}$. In the experimental works, it is common to measure the height of the dense layer via its clarity. Therefore, in this numerical work, we supposed that the height of the current is the place where concentration is equal to 1 % of inlet concentration (like boundary layer approach). The data were non-dimensionalzed by h_0, which is the sluice gate height. In Figure 7, the effects of empirical constant $c_{3\varepsilon}$, or buoyancy term on the current thickness are shown. The current thickness increases as $c_{3\varepsilon}$ increases. Since, buoyancy produces additional turbulent kinetic energy, the entrainment increases; as a result, more dilution occurs in the downstream and the height of the dense layer increases. By observing Figure 7, it can be seen that for these cases, $c_{3\varepsilon} = 0.2$ for k-ω model is in good agreement with the experimental data. After this, all simulations is performed with $c_{3\varepsilon} = 0.2$.

Finally in Figure 8, the non-dimensional velocity profiles computed by k-ω are compared with experimental data of test case 5 (Run 6 of experimental tests) in different locations. Results show that k-ω model can be applied to experimental cases and has an acceptable level of accuracy for estimating the velocity profiles.
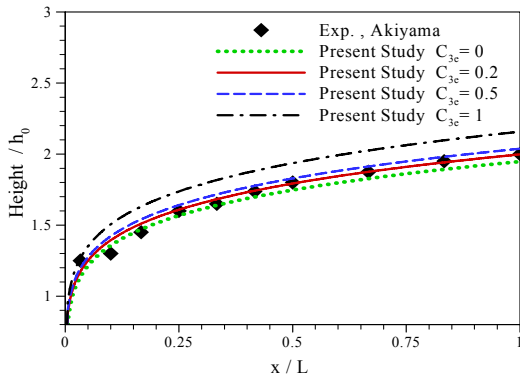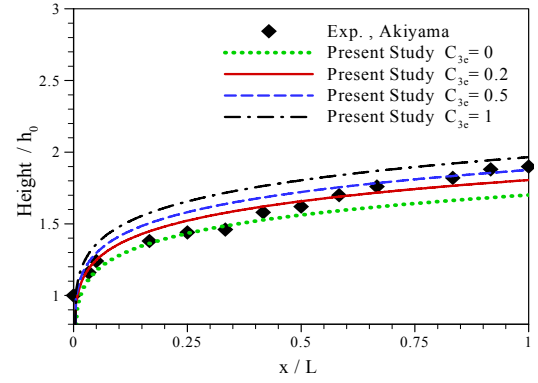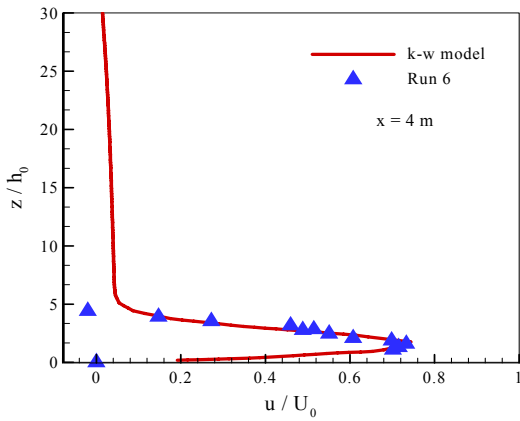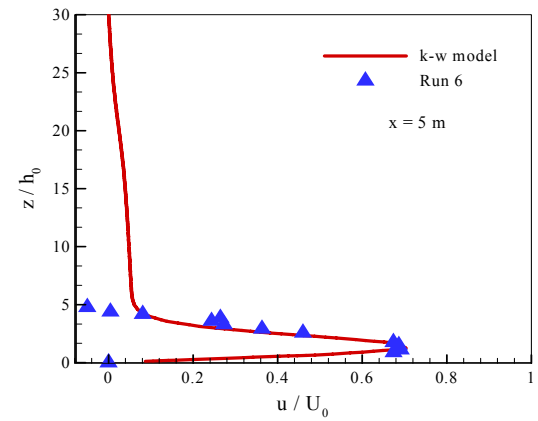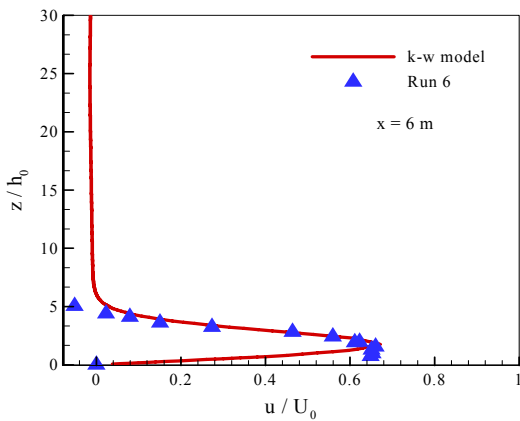
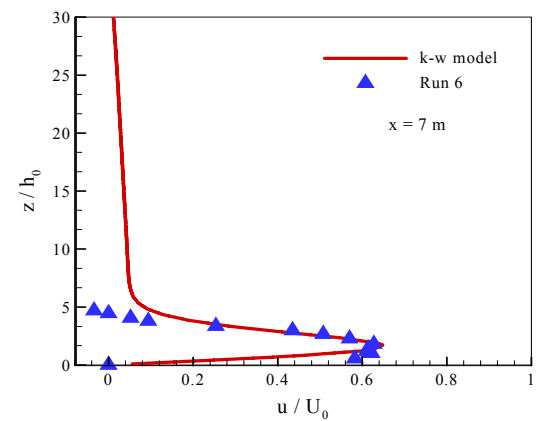**Figure 7**. The effect of $c_{3\epsilon}$ constant on k-ω model, (a) test case 1, (b) test case 2.

Figure 8. Comparison of velocity profile between the numerical result (k-ω model) and experimental result (test case 5) in different locations.

5.2. Results and Discussion In Figure 9a-d the non-dimensional velocity profiles at some downstream locations, using k-ω model and $c_{3\varepsilon} = 0.2$ have been shown. The curves are non-dimensionalized by the inlet velocity (U_0). It can be seen that the maximum velocity occurs near the wall. At the inlet of the channel, due to the existing high inertia force, water entrainment is high. As it can be seen, the maximum magnitude of the velocity at the beginning of the channel is approximately equal to that of the average inlet velocity. By moving along the channel, the magnitude of the velocity decreases sharply and as mentioned before, the point of the maximum velocity shifts upward. It has been shown that with the exception of the region close to the source, the driving force is the component of gravity force parallel to the current direction (x direction).

Comparison between Figure 9 a,b or c,d has shown that the maximum velocity and also its location increases when the inlet velocity rises.

Considering that in the experimental testes concentration profiles is not measured, we compute concentration profile only with the numerical simulation. In Figure 10a-d, the non dimensional concentration profiles at several downstream locations have been shown. The curves are non-dimensionalized by the inlet concentration (C_0). Maximum concentration occurs near the wall and equals the inlet concentration. The vectors of stream-wise velocity have been shown in Figure 11a. It can be seen that the parabolic velocity distribution quickly adapts to the wall-bounded flow, thus producing a maximum velocity very close to the bottom. The interface between the underflow and surrounding water is
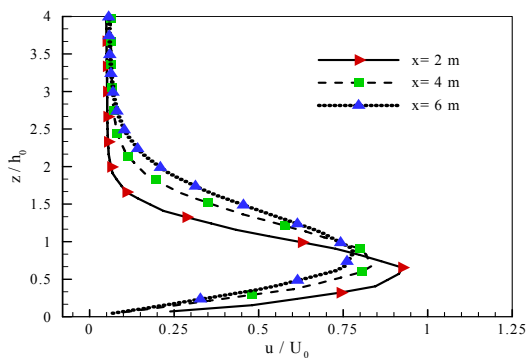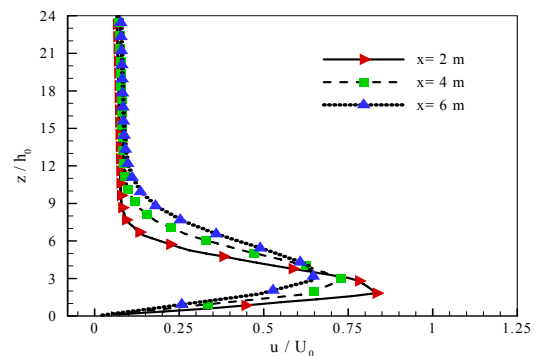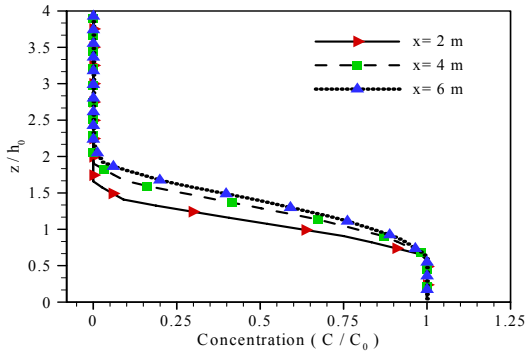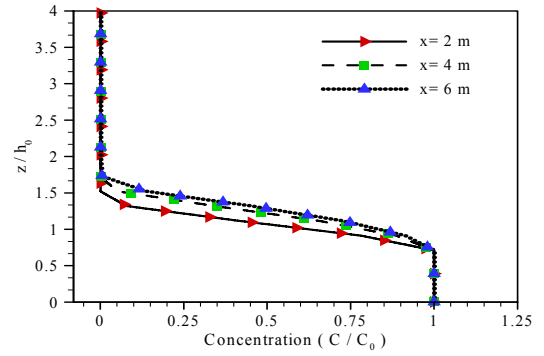

(a)
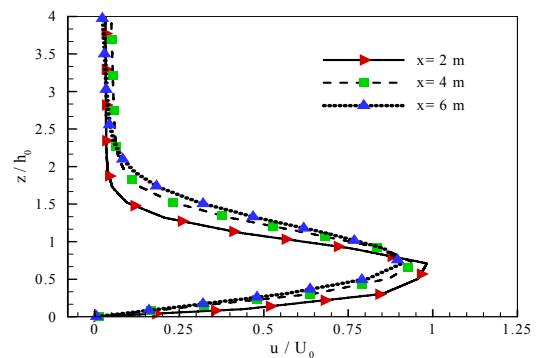
(b)
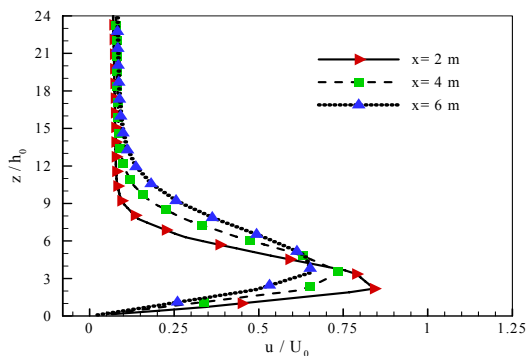
(c)

(d)

Figure 9. Velocity distribution in different location using k-ω model (a) test case 1, (b) test case 2, (c) test case 3 (Run 1), (d)test case 4 (Run 4).

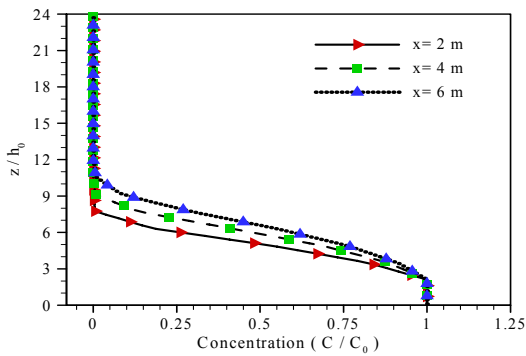observed and it increases along the downstream, which is the result of water entrainment. The contour of concentration in the channel is shown in Figure 11b.
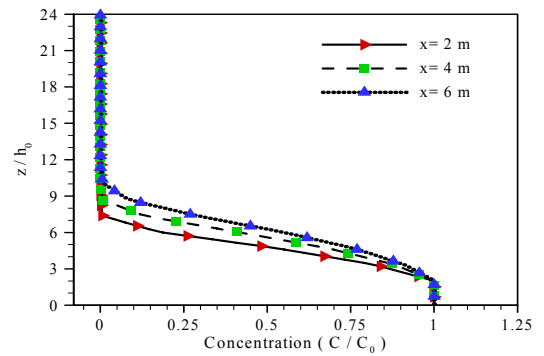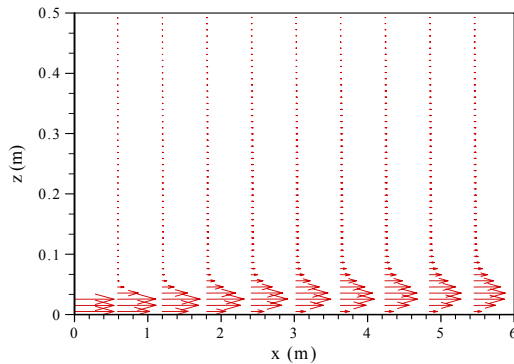

(a)

(b)

(c)
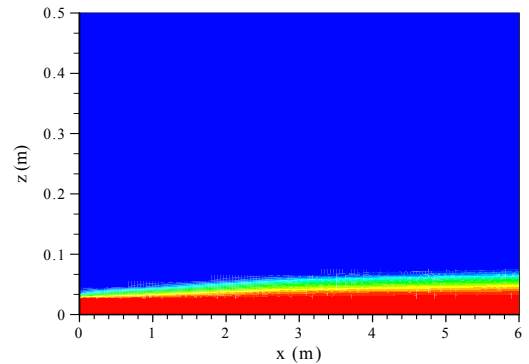
(d)

Figure 10. The concentration profiles in different location using k-ω model, (a) test case 1, (b) test case 2, (c) test case 3 (Run 1), (d) test case 4 (Run 4).

(a)

(b)

Figure 11. (a) Velocity vectors and (b) concentration contorurs that computed by k-ω model for test case 1.

6. CONCLUSION

A series of laboratory experiments were conducted in a channel to study two-dimensional, steady state and turbulent characteristics of a density current. The experimental results show that the maximum and average velocities reduce along the channel. In addition, maximum velocity happens in the upper parts because of the reduction in driving forces of density current and maximum shear stress at the bottom. Besides, for each section, maximum and average velocity and also velocity gradients at the bottom increase with an increase in discharge. In all experiments with different concentrations, it was observed that the thickness of the density current grew with an increase in discharge. It should be mentioned that the magnitude of maximum and average velocity in the x-direction will rise, resulting an increased concentration. It is clear that the increase in density of the current causes an increase in the driving force as well as the velocity. This leads to a decrease in the height of the dense layer, whose effect is seen in the drop of the concentration profiles.

In the second part of the present study, k-ω turbulence model has been applied to simulate the structure of the density current. Momentums, continuity, mass balance and turbulence equations are solved, simultaneously, by SIMPLEC method, without any limited or simplified assumption. The computed heights and velocity profiles of the dense layer were in good agreement with the experimental data.

7. NOMENCLATURE

B_0	Inlet Buoyancy Discharge
b	Width of the Channel
C	Concentration
g'	Gravitational Acceleration
H	Water Depth
h	Density Current Height
h_0	Inlet current Thickness
K	Turbulent Mixing Energy
p	Pressure
p_0	Surface Pressure
Ri_0	Inlet Richardson Number
Re_0	The inlet Reynolds Number
Sc	Schmidt Number
T_{in}	Temperature of the Saline Current in the Mixing Tank
T_s	Temperature of the Surrounding Water in the Channel
U_0	Inlet Velocity
u	X-Velocity
u^*	Shear Velocity
w	Z-Velocity

Greek Symbols

ρ	Density of the Mixture
ρ_s	Salt Density
ρ_w	Water Density
λ	Diffusivity of Fluid
ξ_s	Turbulence Diffusivity
μ	Molecular Viscosity
τ_{ij}	Reynolds Stress Tensor
ω	Specific Dissipation
μ_T	Eddy Viscosity
c_μ, $c_{1\varepsilon}$, $c_{2\varepsilon}$, $c_{3\varepsilon}$	Closure coefficients for k-ω
γ, σ, σ^*, σ_d	Closure Coefficients for k-ω
ε	Turbulent Dissipation Rate
β	Volume Expansion Coefficient
υ	Kinematics Viscosity
κ	Von Karman Constant
θ	Channel Slope Angle in Degree

8. REFERENCES

1. Alavian, V., "Behavior of Density Currents on an Incline", *J. Hydraulic Eng., ASCE*, Vol. 112, No. 1, (1986), 27-42.
2. Simpson, J. E., ''Gravity Currents in the Environment and the Laboratory'', Ellis Harwood, Chi Chester, U.K., (1987).
3. Alavian, V., Jiraka, G. H., Denton, R. A., Johnson, M. C. and Stefan, H. G., "Density Current Enters Lakes and Reservoirs", *J. Hydraulic Eng., ASCE*, Vol. 118, No. 11, (1992), 1464-1489.
4. Ellison, T. H. and Turner, J. S., "Turbulent Entrainments in Stratified Flows", *J. Fluid Mech.*, Vol. 6, (1959), 423-448.
5. Rad, M., "The Deposition of Silt in Reservoirs by Density Current", Ph. D. Thesis, Imperial Coll., London University, U.K., (1976).
6. Garcia, M., "Hydraulic Jumps in Sediment-Driven Bottom Current", *J. Hydraulic Eng., ASCE*, Vol. 119, No. 10, (1993), 1094-1117.
7. Altinakar, M. S., Graft, W. H. and Hopfinger, E. J., "Flow Structure in Turbidity Current", *J. Hydraulic*

Res., Vol. 34, No. 5, (1996), 713-718.

8. Kneller, B. C., Bennett S. J. and McCaffrey, W.D., "Velocity and Turbulence Structure of Density Currents and Internal Solitary Waves: Potential Sediment Transport and the Formation of Wave Ripples in Deep Water", *Sedimentary Geology*, Vol. 112, (1997), 235-250.

9. Akiyama, J. and Stefan, H. G., "Turbidity Current with Erosion and Deposition", *J. Hydraulic Eng., ASCE*, Vol. 111, No. 12, (1985), 1473-1495.

10. Parker, G., "Conditions for the Ignition of Catastrophically Erosive Turbidity Currents", *Mar. Geol.*, Vol. 46, (1982), 307-327.

11. Fukushima, Y., Parker, G. and Pantin, H. M., "Prediction of Ignitive Turbidity Currents in Scripps Submarine Canyon", *Mar. Geol.*, Vol. 67, (1985), 55-81.

12. Parker, G., Fukushima, Y. and Pantin, H. M., "Self Accelerating Turbidity Currents", *J. Fluid Mech*., Vol. 171, (1986), 145-181.

13. Choi, S. C. and Garcia, M., "k-ε Turbulence Modeling of Density Currents Developing Two Dimensionally on a Slope", *J. Hydraulic Eng., ASCE*, Vol. 128, No. 1, (2002), 55-63.

14. Akiyama, J., Ura, M. and Wang, W., "Physical-Based Numerical Model of Inclined Starting Plumes", *J. Hydraulic Eng., ASCE*, Vol. 120, No. 10, (1994), 1139-1157.

15. Firoozabadi, B., Farhanieh, B. and Rad, M., "Hydrodynamics of 2-D Laminar Turbidity Current", *J. Hydraulic Res*., Vol. 41, No. 6, (2003), 623-630.

16. Huang, H., Imran, J. and Pirmez, C., "Numerical Model of Turbidity Currents with a Deforming Bottom Boundary", *J. of Hydraulic Eng., ASCE*, Vol. 131, No. 4, (2005), 283-293.

17. Stacey, M. W. and Bowen, A. J., "The Vertical Structure Density and Turbidity Currents: Theory and Observations", *J. Geophys. Res*., Vol. 93, No. C3, (1988a), 3528-3542.

18. Stacey, M. W. and Bowen, A. J., "The Vertical Structure of Turbidity Currents and a Necessary Condition for Self-Maintenance", *J. Geophys. Res*., Vol. 93, No. C3, (1988b), 3543-3553.

19. Eidsvik, K. J. and Brørs, B., "Self-Accelerated Turbidity Current Prediction Based Upon (k-ε) Turbulence", *Cont. Shelf Res*., Vol. 9, No. 7, (1989), 617-627.

20. Farrell, G. J. and Stefan, H. G., "Mathematical Modeling of Plunging Reservoir Flows", *J. Hydraulic Res*., Vol. 26, No. 5, (1988), 525-537.

21. Firoozabadi, B., Farhanieh, B. and Rad, M., "The Propagation of Turbulent Density Currents on Sloping Bed", *J. Scientia of Iranica*, Vol. 8, No. 2, (2001), 223-235.

22. Imran, J., Kassem, A. and Khan, S. M., "Three-Dimensional Modeling of Density Current. I. Flow in Straight Confined and Unconfined Channels", *J. Hydraulic Research*, Vol. 42, No. 6, (2004), 578-590.

23. Brørs, B. and Eidsvik, K. J., ''Dynamic Reynolds Stress Modeling of Turbidity Currents", *J. Geophysics Res*., Vol. 97, No. C6, (1992), 9645-9652.

24. Launder, B. and Sharma, B., "Application of the Energy-Dissipation Model of Turbulence to the Calculation of Flow near a Spinning Disc", *Letters in Heat Mass Transfe*, Vol. 1, (1974), 131-138.

25. Khakzad, N., Firoozabadi, B. and Farhanieh, B., "Qualitative Numerical Investigation of Steady Buoyancy Reserving Density Currents Down an Incline Using v^2-f Turbulence Model", *J. Fluids Eng., ASME*, No. 9, Vol. 129, (2007), 1172-1178.

26. Launder, B. E. and Rodi, W., "The Turbulent Wall Jet-Measurement and Modeling", *Annual Review of Fluid Mechanics*, Vol. 15, (1983), 429-33.

27. Ljuboja, M. and Rodi, W., "Calculation of Turbulent Wall Jets with an Algebraic Reynolds-Stress Model", *J. Fluids Eng., ASME*, Vol. 102, (1980), 350-356.

28. Kechiche, J., Mhiri, H., Le Palec, G. and Bournot, P., "Application of Low Reynolds Number k-epsilon Turbulence Models to the Study of Turbulent Wall Jets", *International J. Thermal Sciences*, Vol. 43, No. 2., (2004), 201-211.

29. Wilcox, D. C., "Progress in Hypersonic Turbulence Modeling", *J. AIAA*, Vol. 109, (1987), 156-160.

30. Lyn, D. A., Stamou, A. I. and Rodi, W., "Density Currents and Shear-Induced Flocculation in Sedimentation Tanks", *J. Hydraulic Eng., ASCE*, Vol. 118, No. 6, (1992), 849-867.

31. Parneix, S., Durbin, P. and Behnia, M., "Computation of 3-D Turbulent Boundary Layer Using the v^2-f Model Flow", *Turbulence and Combustion*, Vol. 60, (1998), 19-46.

32. Durbin, P. A. and Patterson B. A., "Statistical Theory and Modeling for Turbulent Flow", John Willey and Sons LTD, New York, U.S.A., Vol. 2, (2001), 109-131.

33. Rodi, W., "Examples of Calculation Methods for Flow and Mixing in Stratified Fluids", *J. Geophys. Res*., Vol. 2, No. C3, (1987), 5305-5328.

34. Fukushima, Y., and Hayakawa, N., "Analysis of Inclined Wall Plume by the k-ε Turbulence Model", *J. Appl. Mech*., Vol. 57, (1990), 455-465.

35. Ferziger, J. H. and Peric, M., "Computational Methods for Fluid Dynamics", Springer, Berlin, Germany, (1996).

36. Rhie, C. M. and Chow, W. L., "Numerical Study of the Turbulent Flow Past on Airfoil with Trailing Edge Separation", *J. AIAA*, Vol. 2, (1983), 1527-1532.